Journal of Materials Chemistry B

ROYAL SOCIETY OF CHEMISTRY

PAPER

View Article Online
View Journal

Cite this: DOI: 10.1039/d5tb02688a

Graphene-based porous hydrogels with a tunable piezoresistive response for wearable strain sensing

Nishadi M. Bandara, [a] Khandaker Umaiya,[a] Michael J. Joyce, [a] Cesar E. Gouveia[b] and Douglas H. Adamson *[ab]

Received 1st December 2025,
Accepted 3rd April 2026

DOI: 10.1039/d5tb02688a

rsc.li/materials-b

This study reports the synthesis of porous hydrogels templated by self-assembled, percolating graphene networks formed through the spontaneous exfoliation of graphite at oil–water interfaces. The resulting graphene-stabilized emulsions yield an open-cell hydrogel architecture that enables efficient stress-dependent modulation of electrical pathways. Compression testing and electrical characterization revealed a pronounced reduction in resistance under strain, producing a robust and reliable piezoresistive response with a gauge factor of approximately 13 at 5% strain. Cyclic compression–relaxation experiments confirmed the high reversibility and stability of both the mechanical and piezoresistive responses. Crosslinking density strongly influenced sensitivity, enabling tunable piezoresistive performance suited for real-time motion monitoring. When mounted on a finger joint, the hydrogel exhibited smooth changes in resistance (35%–70%) as the bend angle increased from 30° to 90°, with excellent signal stability under static deformation. Additionally, the hydrogels demonstrated strong absorptive capabilities, enabling efficient removal of organic dyes and metal ions through repeated compress–release cycles. Collectively, the combination of elasticity, electrical conductivity, and sorption functionality positions these graphene-templated hydrogels as promising candidates for wearable sensing technologies and environmental remediation applications.

Introduction

Graphene, a single layer of carbon atoms arranged in a two-dimensional honeycomb lattice, exhibits extraordinary properties such as high thermal conductivity,[1] electron mobility,[2] surface area,[3] mechanical strength,[4] and piezoresistivity,[5] which make it a promising material in fields ranging from catalysis and transistors to energy storage and biomedical applications.[6–8] These properties also suggest that it is an ideal candidate for enabling strain sensing in composite materials.[9]

Strain sensors, which detect changes in electrical resistance in response to mechanical deformation, play a pivotal role in applications such as wearable health monitoring,[10] electronic skin,[11] soft robotics,[12] and human–machine interfaces.[13] Among the primary types of strain sensors, piezoelectric,[14–16] piezoresistive,[17–19] and triboelectric,[20,21] piezoresistive sensors stand out due to their simplicity in design, low cost, and ease of signal interpretation.[22] Hydrogels, with their soft mechanical properties, high water content, and flexibility, are increasingly favored as substrates for piezoresistive sensors, particularly for applications requiring skin-like adaptability.[23–26]

Hydrogels are three-dimensional, water-swollen polymer networks formed by hydrophilic monomers that can respond dynamically to environmental stimuli, including strain.[27–29] The polymer network's structure consists of covalent and non-covalent bonds, such as hydrogen bonding, electrostatic, and hydrophobic interactions, that enable both elasticity and responsiveness, crucial for adaptable strain-sensing materials.[30,31] By integrating conductive materials such as graphene, hydrogels form percolated conductive networks that translate mechanical strain into electrical signals, thereby enabling piezoresistive sensing.[32,33]

Previous investigations of graphene-based conductive hydrogels have used graphene oxide (GO) or reduced graphene oxide (rGO) in their synthesis. However, GO's reduced conductivity and rGO's hydrophobicity and tendency to aggregate result in challenges to achieving high electrical conductivity and elasticity in the hydrogel matrix.[34] The study we present here addresses these challenges through a novel solvent interfacial trapping method (SITM), where pristine, unoxidized graphene serves as a 2D surfactant, stabilizing a water-in-oil emulsion.

At ambient temperature (20 °C), the surface energy of graphene ($\sim$55 mN m^{-1}) lies between the surface tensions of water (72.9 mN m^{-1}) and heptane (20.1 mN m^{-1}), resulting in a positive spreading parameter (S = 6.6 mN m^{-1}).[35,36] This

[a] Department of Chemistry, University of Connecticut, Storrs, Connecticut, USA. E-mail: douglas.adamson@uconn.edu
[b] Polymer Program, Institute of Materials Science, University of Connecticut, Storrs, Connecticut, USA

positive value indicates that graphene sheets are spontaneously driven to spread at the liquid–liquid interface, thereby reducing the system's overall free energy.[37,38] Furthermore, mechanical agitation, such as shaking, increases the interfacial area, thereby promoting further exfoliation of graphene. This agitation leads to the formation of an emulsion, with water droplets dispersed within the heptane phase, and graphene sheets coating their surfaces.[39] In this process, if a monomer is used as the oil phase, subsequent polymerization of the continuous phase results in the formation of water-filled spherical cavities lined with a layer of overlapping graphene sheets and surrounded by polymer.[40]

Graphene forms water-in-oil emulsions as a result of graphene's intrinsic hydrophobicity, and following Bancroft's rule, the phase in which the emulsifier (graphene) is more soluble becomes the continuous phase.[41] This has traditionally led to the fabrication of open-cell graphene–polymer foams where the oil phase contained monomers. However, recent innovations have focused on modifying graphene's interfacial properties to broaden SITM's structural options. Specifically, the incorporation of polyphenolic compounds, such as tannic acid (TA), has enabled a phase inversion from water-in-oil to oil-in-water emulsions.[42] Tannic acid, which possesses multiple galloyl groups, interacts with the sp^2-hybridized carbon atoms of graphene through π–π stacking, significantly enhancing the hydrophilic character of the graphene sheets.[43,44] This interaction reduces graphene's affinity for the oil phase, causing it to preferentially stabilize oil droplets in an aqueous continuous phase, inverting the emulsion structure.

By employing tannic acid in the aqueous phase, inverted-SITM enables the graphene stabilization of oil-in-water emulsions and the polymerization of monomers such as butyl acrylate in the dispersed phase. This has led to the fabrication of compressible, conductive microspheres, in contrast to the open-cell structures produced *via* traditional SITM.[42] The success of this approach inspired the exploration of water-soluble monomers in the continuous aqueous phase. Polymerization of aqueous phase monomers in the oil-in-water emulsions yields hydrogels, marking the evolution from open-cell graphene–polymer foams to porous microspheres to soft functional materials, featuring a network of overlapping graphene embedded within a polymer matrix that adapts under compressive stress, enhancing conductive pathways and enabling piezoresistive sensitivity.

Current challenges for conductive hydrogels include limited sensitivity and poor long-term stability, which restrict practical applications.[45] Recent organo-hydrogel strategies reduce internal friction and entanglements, yielding low-hysteresis and fast strain sensing.[46] Building on this progress, we employ percolated graphene networks to enable piezoresistive readout and angle-stable responses. In this investigation, we evaluate the material's mechanical and piezoresistive responses under varying crosslinking densities, demonstrating its applicability as a wearable sensor, with Table S1 comparing its properties to those previously reported in the literature. Combining elasticity, electrical conductivity, and electrical stability, this hydrogel design offers a solution for wearable sensing.

Results and discussion

Hydrogel synthesis and morphology

The solvent interfacial trapping method (SITM) employed here enables the spontaneous exfoliation of graphite at oil–water interfaces, resulting in a graphene-stabilized emulsion. Using tannic acid during graphene exfoliation enhances the graphene's hydrophilicity, thereby facilitating emulsion inversion to form stable oil-in-water emulsions conducive to hydrogel formation. This inversion is essential for the subsequent formation of a poly(*N*-(hydroxymethyl) acrylamide) (PHMA) hydrogel network, in which the water-soluble HMA monomer polymerizes to form a 3D matrix containing interconnected graphene-coated spheres. Shown schematically in Fig. 1a, the polymerization of HMA monomer with the crosslinker ethylene glycol dimethacrylate and the initiator ammonium persulfate results in an interstitial PHMA hydrogel encapsulating a 3D network of graphene-coated spheres.

SEM analysis (Fig. 1b and c) reveals an open-cell foam structure, with individual hydrogel cells bordered by graphene, which facilitates electrical conductivity through continuous graphitic pathways. Each cell of the hydrogel foam is lined with an overlapping film of graphene sheets, which are in contact with neighboring cells. This provides a percolating network of graphene, leading to good electrical conductivity. Connecting these cells are windows, where only a thin layer of graphene separates the contents of the spheres. Windows, or openings, between the cells enables the removal of the dispersed phase, forming an open-cell, electrically conductive hydrogel foam.

Mechanical properties and elasticity of the graphene-based hydrogel

Fig. 2 shows the compressive stress–strain curves for 50% compress–release cycles of hydrogel samples with a 2.8% weight graphite loading and increasing monomer-to-crosslinker ratios. The measurements were made using an Instron as shown in Fig. S1. The loading curve of the first compressive cycle differed from those of subsequent cycles in all cases. The first compression cycle expelled residual water, while subsequent cycles demonstrated reproducible elasticity with a consistent stress level at 50% compression. This elastic performance was attributed to the dynamic hydrogen bonding in poly(HMA), which allowed the hydrogel to dissipate energy without fracturing the covalent network.[22] Additionally, compressive stress remained near zero for each loading cycle until approximately 10% compression was reached (except for the first loading), due to the hydrogel's volume decrease following water removal during the initial compression. Additional compressions of 50% maintained similar compressive stress across the rest of the cycles, with little to no hysteresis, demonstrating the hydrogel sponge's reversible elastic behavior.[47]

Covalent crosslinking enhanced the mechanical properties of the hydrogels, increasing the graphene-lined spheres' ability to resist deformation and distribute the applied force throughout the structure. The impact of crosslinking was studied by

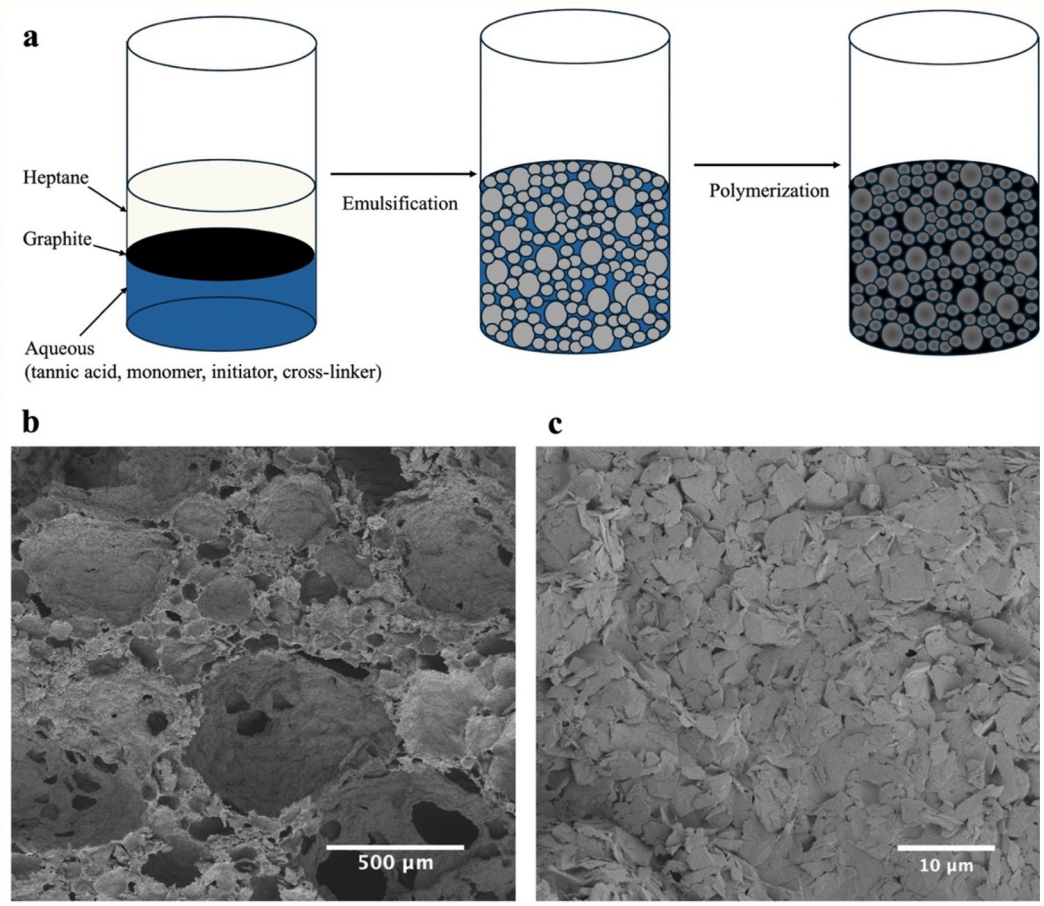

Fig. 1 (a) Schematic showing the preparation of a hydrogel from a water-in-oil emulsion. SEM images of the hydrogel (b) at low magnification showing open-cell foam with windows and (c) at high magnification showing the overlapping graphene sheet lining the cells.

fabricating materials with decreasing monomer-to-crosslinker molar ratios. Fig. 2a–e show the stress–strain curves with molar ratios of 60 : 1, 30 : 1, 20 : 1, 15 : 1, and 7.5 : 1, respectively. As the monomer:crosslinker ratio decreased or, in other words, as the extent of covalent crosslinking increased, the compressive stress required to reach 50% compression increased, as summarized in Fig. 2f. Below a monomer-to-crosslinker ratio of 7.5 : 1, the hydrogels started to crumble and break upon compression.

Notably, a small, precisely reproduced hitch was observed during the compression cycles. We attributed this hitch to a particle-jamming mechanism, as the graphene-lined cells of the foam moved past one another during compression. Although we do not have direct evidence of particle jamming, the hitch became apparent at a similar compression (35%) for hydrogels with less extensive crosslinking and disappeared at higher crosslink densities. Jamming is indicated because, at lower polymer stiffness (a large monomer-to-crosslinker ratio), the graphene-coated spheres carry much of the load and are expected to slip past one another rather than compress. At higher polymer stiffness (small monomer-to-crosslinker ratio), the polymer carries much of the load, and the spheres can no longer move past one another; thus, the hitch in the stress/strain curve did not appear as the sphere deformed.

In addition to investigating the effect of crosslink density, we examined the impact of increasing the amount of graphite added. The samples were subjected to 50% multi-compress-release cycles, as shown in Fig. S2 and summarized in Fig. 3, and the increased graphite loading resulted in increased compressive strength. However, above a 3.5% graphite loading, the hydrogel fractured during the initial compression cycle. The explanation for this phenomenon stems from previous work that found that increased graphite loading resulted in a closed-cell foam that retained the dispersed phase.[39] These incompressible cells could not deform under hydrogel compression. Instead, the hydrogel tore under stress.

Smaller amounts of graphite also proved problematic, as we were unable to obtain hydrogel samples for graphite weight percentages below 1.9%. This appeared to be due to the graphite-to-tannic acid ratio. A previous study that used tannic acid to stabilize a graphene emulsion found that an excess of tannic acid relative to graphite led to emulsion instability.[48] Therefore, preparing composites outside the investigated range would require adjusting the tannic acid concentration in the aqueous phase as the graphite amount varied. To avoid

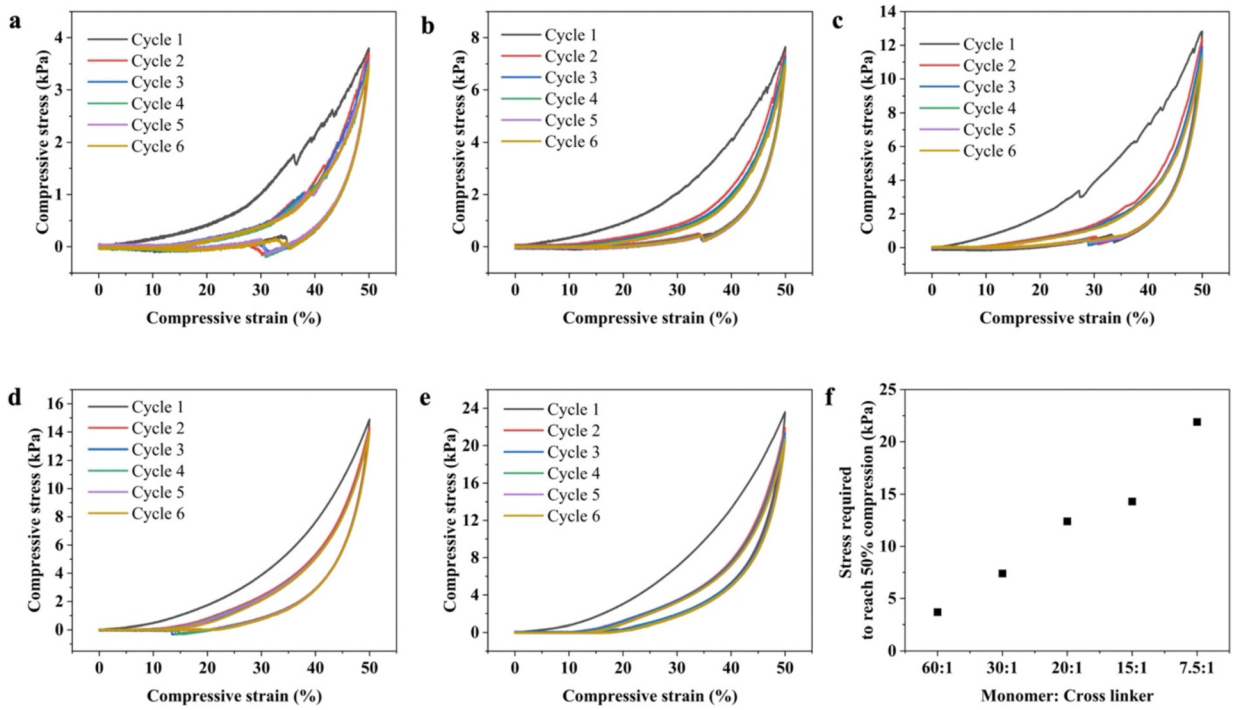

Fig. 2 Multi 50% compress–release cycles of hydrogels with monomer:crosslinker molar ratios of (a) 60 : 1, (b) 30 : 1, (c) 20 : 1, (d) 15 : 1 and (e) 7.5 : 1, respectively. (f) Stress required to reach 50% compression for hydrogel samples with different monomer:crosslinker molar ratios.

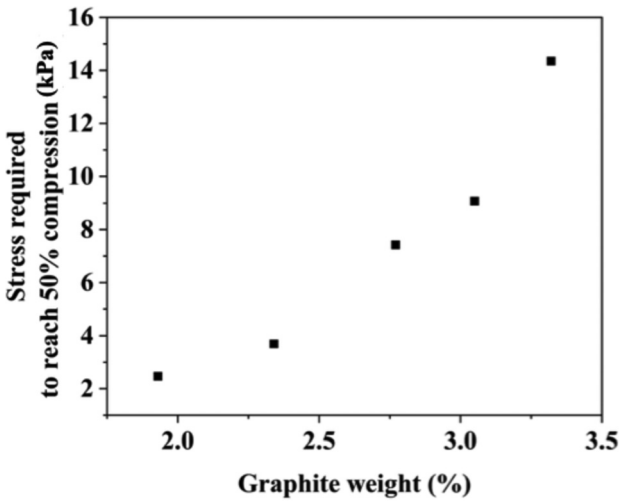

Fig. 3 Stress required to reach 50% compression for hydrogel samples with different graphite weight percentages.

changing two parameters simultaneously, we limited ourselves to graphite weight percentages that formed stable emulsions with the 1 mg mL^{-1} tannic acid solutions.

Piezoresistive response

To characterize the piezoresistive properties of the PHMA graphene hydrogel foam, the foam was placed between two parallel copper electrodes, and copper wires were connected to them. The experimental setup is shown in Fig. S3. As shown in Fig. 4a, the piezoresistive response of hydrogels made with different crosslink densities was investigated as a function of compression. The change in resistance was plotted as per the following formula:

$$\frac{\Delta R}{R_0}(\%) = \frac{(R - R_0)}{R_0} \times 100 \quad (1)$$

where R_0 and R denote the resistance without and with applied stress, respectively. When the sponge was compressed, the electrical resistance decreased. This relationship between the change in resistance and the strain was found to depend on the material's crosslink density, with the materials that displayed what we hypothesized to be particle jamming in Fig. 2 showing a much greater and more abrupt change in resistance under compression.

The sudden release of jamming that lead to a hitch in the stress/strain curves correlated with a sharp change in resistance as the number of contact points between the spheres changed with a change in the packing state. The consistency of the hitch position at ~35% compression across three crosslink densities, combined with the abrupt drop in resistance at the same strain level in low-crosslink-density samples, is consistent with a sudden increase in graphene-to-graphene contact area expected if loosely packed spheres transitioned to a jammed state.

Fig. 4b plots the hydrogel's gauge factor (GF) as a function of compressive strain at four different crosslink densities. The GF is defined as the ratio of the relative change in electrical resistance ($\Delta R/R_0$) to the mechanical strain (ε), as shown in eqn (2).

$$GF = [\Delta R/R_0]/\varepsilon \quad (2)$$

The GF was dramatically greater for the softer samples when the monomer:crosslinker ratio was above 20 : 1. These GF

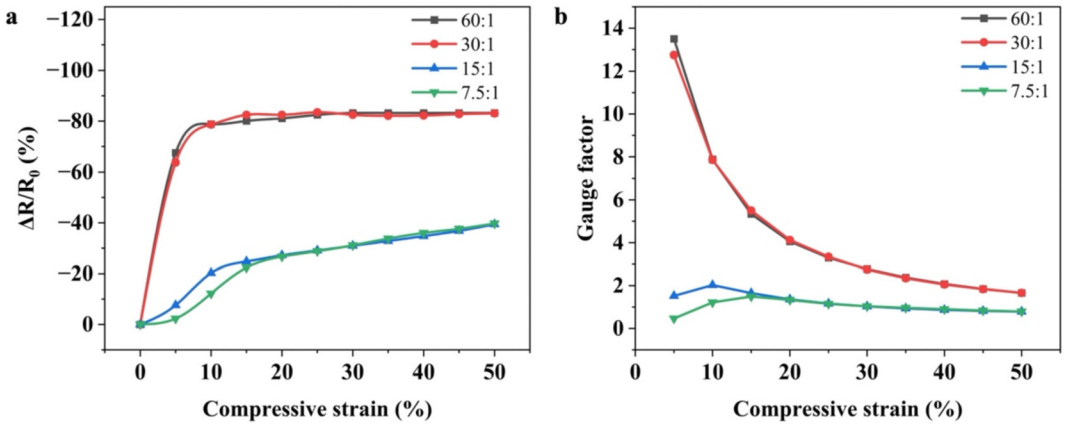

Fig. 4 (a) The percentage decrease of resistance with compressive strain and (b) variation of gauge factor with compressive strain for samples with different monomer : crosslinker molar ratios of 60 : 1, 30 : 1, 15 : 1, and 7.5 : 1.

results at low strain showed that the samples with lower degrees of crosslinking were more sensitive to compression, with a gauge factor of 13 at 5% strain. This value of the gauge factor is significantly higher than that reported for piezoresistive materials[47,49–52] (Table S1), suggesting that our hydrogel exhibits superior sensitivity.

The cycling stability of our hydrogel was tested as shown in Fig. S4. The reproducibility of resistance variation over 100 loading/unloading cycles indicates the reliability of the hydrogel sponges as pressure sensors. While the 100-cycle test confirms stable and reproducible piezoresistive performance, extended durability testing under realistic wearable conditions, including prolonged cycling, perspiration exposure, and temperature variation, will be an important consideration for translating these materials toward practical wearable devices and is a direction for future work.

Hydrogels with increasing crosslink density were compressed and released in multiple ten-second cycles. The change in resistance over time was plotted and compared with the change in compression. Fig. 5a–e demonstrate that the sensitivity of resistance to strain significantly diminishes with increasing crosslink density. Furthermore, the reversibility of the piezoresistive effect shows no apparent hysteresis. Similar measurements at 40% strain are shown in Fig. S5. Fig. 5f summarizes the results and compares the 20% and 40% compression rates. Somewhat surprisingly, we found that at low crosslink density, there was very little difference in the change in resistance when the strain was doubled. This

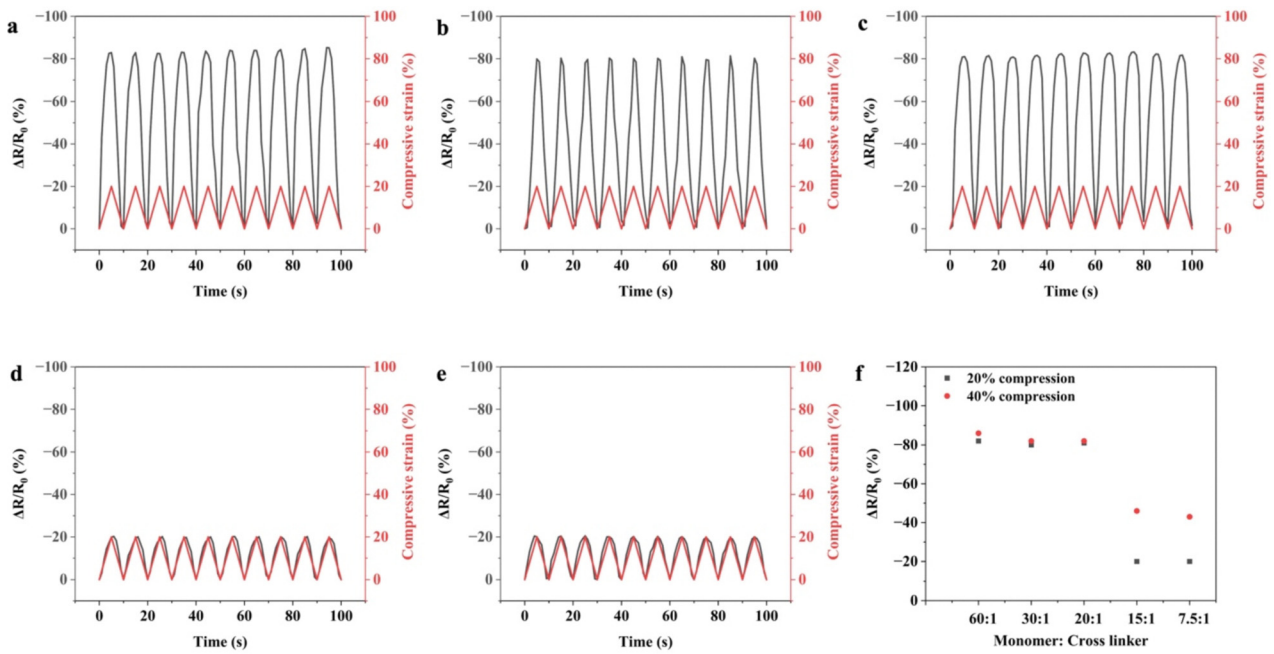

Fig. 5 Change of electrical resistance for hydrogel sensors made with monomer : crosslinker molar ratios of (a) 60 : 1 (b) 30 : 1 (c) 20 : 1 (d) 15 : 1 and (e) 7.5 : 1 undergoing 20% compressions and relaxations at regular time intervals. (f) Summary of the effect of 20% and 40% compressions on resistance change of hydrogels made with different molar ratios.

suggests that the spheres adopt a denser packing arrangement under strain, and that further strain does not alter it. Thus, fundamentally different mechanisms underlie changes in resistance, depending on the hydrogel's stiffness.

To visually demonstrate this strain-sensitive conductivity, a 3 V power supply and a blue LED were connected in a circuit with the hydrogel. The hydrogel underwent a gradual compression from 0% to 50%, followed by a gradual release at the same rate. As shown in Fig. S6, the intensity of blue light increased as the hydrogel was compressed, whereas the brightness gradually diminished as the hydrogel was released.

Hydrogel as a motion detector

One application of piezoresistive materials is the detection of human motion. We demonstrated the utility of our hydrogel for this application by attaching it to wrist, finger, and elbow joints using adhesive tape. The chosen hydrogel had a graphite weight percentage of 2.8%, a monomer:crosslinker ratio of 30 : 1, and was sandwiched between two copper electrodes. Both electrodes were connected to a digital multimeter to measure the changes in resistance. The sensing response, or the relative change in resistance, was calculated using eqn (1), where R_0 and R were the sensor's original resistance and the resistance after bending, respectively.

The real-time change of the resistance during the bending of the wrist, elbow, and finger is shown in Fig. 6a–c. When bent, the strain sensor is compressed, resulting in a decrease in resistance. The hydrogel-based sensor exhibited rapid and repeatable responses to consecutive bend-release cycles, indicating the durability and stability of the hydrogel sensors. As the wrist joint bent and released slowly and quickly, the electrical response of the hydrogel varied accordingly, as shown in Fig. 6a. Moreover, the hydrogel's resistance remained stable during the bending-holding and relaxation-holding processes at the wrist joint, indicating its electrical stability. This stability is shown in Fig. 6d. As the finger bent at increasing angles, ranging from 0° to 90°, the resistance of the hydrogel decreased with increasing compression and remained stable as long as the compression was maintained. Such stability is necessary for many sensor applications.

Our human motion monitoring study demonstrated several distinctive features compared to previous reports. The resistance remains stable when the device is held at a specific bending angle. Also, the material exhibits a rapid response across various motion speeds and maintains a strong correlation with the bend

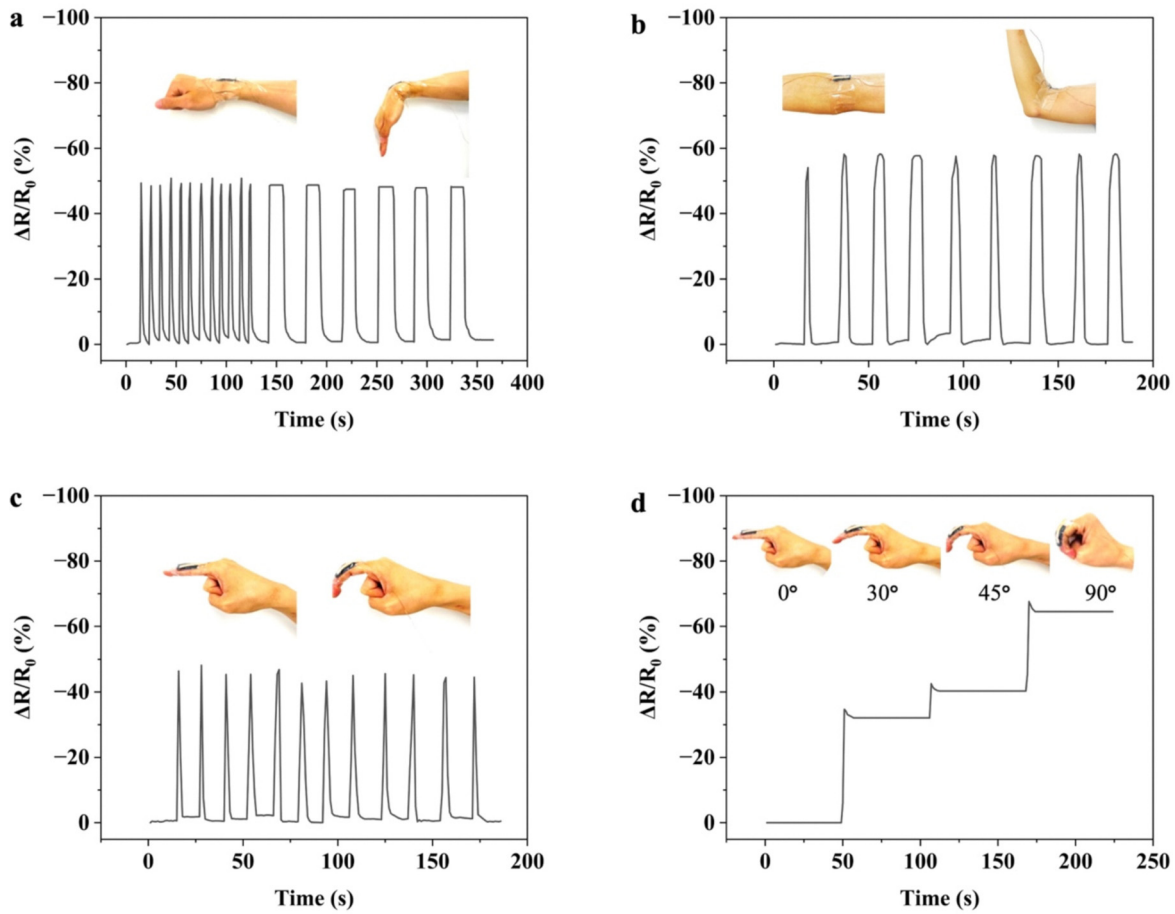

Fig. 6 Relative resistance changes of the sensors *versus* time for real time monitoring of various human motions: bending and release of the (a) wrist joint, (b) elbow joint and (c) finger joint. (d) Resistance change of the hydrogel sensor in response to different bending angles of the finger.

angle. Finally, our material shows negative piezoresistive behavior. Unlike many graphene-based sensors that exhibit increased resistance under strain, our sensors display decreased resistance, offering advantages in signal-to-noise ratio and power efficiency, making the material highly promising for practical wearable sensing applications.

This negative piezoresistive behavior contrasts with that of previously reported elastomer foams templated by graphene-stabilized water-in-oil emulsions, in which polymerization occurred in the oil phase. In those cases, resistance increased with compression and then returned to its original level when the compression was released.[53] The explanation for this difference between the previously reported elastomers and the hydrogel presented here stems from the different morphologies of the foams, where the oil phase of the water-in-oil emulsion was polymerized (previous work) rather than the aqueous phase of the oil-in-water emulsion (current work). The interfacial exfoliation of graphite to graphene results in graphene being present on the oil side of the oil/water interface.[54] This means that the graphene is nearly entirely embedded in the polymer after polymerization if the oil phase is polymerized. In the present system, the graphene ends up at the surface of the elastomeric polymer synthesized in the aqueous phase. This permits more efficient contact between the graphene shells during compression. This increased contact drives the decrease in resistivity response during compression. In contrast, the increase in resistivity under compression in the previous materials was driven almost entirely by sphere deformation, leading to gaps in the conductive network.[55,56]

Absorptive properties of the elastic hydrogel

Finally, the hydrogel's elasticity was applied to effectively remove dye molecules from aqueous solutions. As shown in Fig. 7a, compressing and releasing the hydrogel at regular time intervals while submerged in an aqueous dye solution significantly increased the amount of dye removed from the solution compared to simple diffusion. As expected, the hydrogel subjected to periodic mechanical stimulation exhibited substantially faster dye absorption than the sample left to equilibrate without external stimulation. This enhanced sorption performance arises from the intrinsically high specific surface area of graphene and the strong π–π interactions between the dye molecules and the graphene.[52] In addition, the robust mechanical elasticity of the hydrogel enables repeated compression–relaxation cycles without structural failure, thereby facilitating accelerated mass transfer and continuous pollutant uptake.

The hydrogel's elasticity and electrical conductivity were subsequently utilized to facilitate the removal of metal ions from aqueous solutions, using Cu^{2+} as a model cation. A control sample was immersed in the Cu^{2+} solution for 30 minutes, while experimental samples underwent 15 compression–relaxation cycles at regular intervals over the same period. Here, four samples were additionally subjected to external electrical potentials while undergoing mechanical stimulation. As shown in Fig. 7b, applying an electrical potential significantly enhanced Cu^{2+} removal, with higher voltages corresponding to greater uptake. We hypothesize that this enhanced removal resulted from the reduction of Cu^{2+} within the hydrogel matrix under the applied electrical potential.

The absorptive properties of the hydrogel are presented to illustrate the multifunctional potential of the graphene-based porous architecture. The dye and metal-ion absorption results demonstrated proof-of-concept functionality enabled by the high surface area of graphene, the hydrogel's electrical conductivity, and its mechanical elasticity, which allows accelerated mass transfer through compression–relaxation cycling. Systematic studies of reusability, including desorption kinetics and regeneration over multiple absorption–desorption cycles, are being explored in ongoing work.

Conclusion

In this work, we synthesized graphene-based hydrogels using the solvent interfacial trapping method, producing a mechanically resilient and electrically responsive porous architecture. The fabrication process is economical, scalable, and environmentally

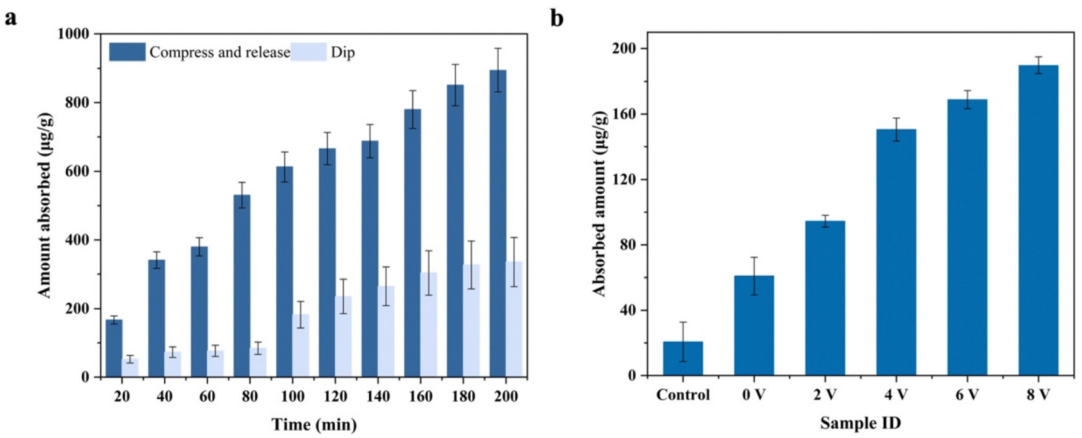

Fig. 7 (a) Comparison of the dye absorption capability of the hydrogel samples with time. (b) Comparison of the Cu^{2+} absorption capability of each sample after 30 minutes.

friendly, while the resulting materials exhibit tunable piezoresistive properties. The compressive stress required to reach 50% strain ranged from 4 kPa to 24 kPa, depending on crosslink density. A continuous network of graphene-coated microspheres enables efficient stress-dependent modulation of conductive pathways, and the piezoresistive sensitivity is strongly governed by crosslinker concentration. The hydrogels maintain stable electrical resistance responses over repeated compression–release cycles, confirming reliable and reproducible performance. Importantly, the materials achieve a gauge factor of ~13 at 5% strain and demonstrate excellent capability for monitoring human joint motions, including wrist, elbow, and finger bending. Additionally, the material exhibited strong adsorptive capacity, enabling efficient removal of dye molecules and metal ions *via* cyclic compression. Collectively, these results highlight graphene-based PHMA hydrogels as a versatile platform for next-generation wearable sensors and multifunctional environmental remediation systems.

Experimental

Materials

Natural graphite with a flake size of 3–5 μm (micro 850) was obtained from Ashbury Graphite Mills, Inc. *N*-(Hydroxymethyl)-acrylamide (TCI America, 98.0%), ethylene glycol dimethacrylate (TCI America, 97.0%), tannic acid (Alfa Aesar), ammonium persulfate (Fisher, 98%), and *n*-heptane (Fisher, 99%) were all used as received.

Sample preparation

A glass jar (240 mL) was loaded with 30 mL of a 10% (by weight) *N*-(hydroxymethyl)acrylamide aqueous solution, 0.196 mL ethylene glycol dimethacrylate crosslinker (for a 30 : 1 monomer to crosslinker ratio), 30 mg tannic acid (1 mg tannic acid per mL water), and 0.14 g ammonium persulphate initiator. The components were mixed well. Next, 30 mL of heptane was added, followed by 1.45 g of graphite. This procedure results in a 2.8 wt% graphite-loaded hydrogel. The jar was then sealed and shaken for two minutes using a bubble tea shaker (Happybuy Milk Tea shaker, 320 rpm). Finally, the jar was placed in a convection oven (Blue M, Stabil-Therm) at 65 °C for two hours to polymerize. Then, the sample was removed from the jar, and the bulk poly(hydroxymethylacrylamide) was separated, thoroughly washed to remove residuals, and subsequently used for characterization.

Characterization

The morphology of the dried hydrogel was observed under a scanning electron microscope (FEI Nova SEM450). Compression testing was performed using an Instron Model 5869 with a 5 kN load cell. Piezoresistivity was measured using a digital multimeter (Amprobe 38XR-A), and the data were recorded using Amprobe software. The amount of dye absorbed was calculated by measuring the remaining dye at each time interval using UV-visible spectroscopy (Lambda 1050, PerkinElmer). The amount of Cu^{2+} removed from the solution within 30 minutes was calculated by determining the amount remaining at the end of 30 minutes using atomic absorption spectroscopy (AAS) (PerkinElmer Analyst 200).

All mechanical and piezoresistive measurements were performed in triplicate (minimum) for each composition. The compressive stress at 50% strain showed a coefficient of variation of less than 15% across samples of the same composition, and piezoresistive response curves were qualitatively consistent.

Conflicts of interest

The authors declare no conflicts of interest.

Data availability

The data supporting the findings of this study are available within the article and its supplementary information (SI). See DOI: https://doi.org/10.1039/d5tb02688a.

Additional raw data or analysis files are available from the corresponding author upon request.

Acknowledgements

The authors gratefully acknowledge funding for this work provided by the National Science Foundation (NSF) through the DMREF program (grant number DMR1535412) and by the U.S. Department of Agriculture (USDA) (project award number 221470).

References

1 A. A. Balandin, S. Ghosh, W. Bao, I. Calizo, D. Teweldebrhan, F. Miao and C. N. Lau, Superior Thermal Conductivity of Single-Layer Graphene, *Nano Lett.*, 2008, **8**(3), 902–907, DOI: 10.1021/nl0731872.

2 M. Orlita, C. Faugeras, P. Plochocka, P. Neugebauer, G. Martinez, D. K. Maude, A.-L. Barra, M. Sprinkle, C. Berger, W. A. De Heer and M. Potemski, Approaching the Dirac Point in High-Mobility Multilayer Epitaxial Graphene, *Phys. Rev. Lett.*, 2008, **101**(26), 267601, DOI: 10.1103/PhysRevLett.101.267601.

3 A. Peigney, Ch Laurent, E. Flahaut, R. R. Bacsa and A. Rousset, Specific Surface Area of Carbon Nanotubes and Bundles of Carbon Nanotubes, *Carbon*, 2001, **39**(4), 507–514, DOI: 10.1016/S0008-6223(00)00155-X.

4 C. Lee, X. Wei, J. W. Kysar and J. Hone, Measurement of the Elastic Properties and Intrinsic Strength of Monolayer Graphene, *Science*, 2008, **321**(5887), 385–388, DOI: 10.1126/science.1157996.

5 S. Chun, Y. Choi and W. Park, All-Graphene Strain Sensor on Soft Substrate, *Carbon*, 2017, **116**, 753–759, DOI: 10.1016/j.carbon.2017.02.058.

6 K. M. Janavika and R. Prakash Thangaraj, Graphene and Its Application: A Review, *Mater. Today: Proc.*, 2023, S2214785323030821, DOI: 10.1016/j.matpr.2023.05.446.

7 V. B. Mbayachi, E. Ndayiragije, T. Sammani, S. Taj, E. R. Mbuta and A. U. Khan, Graphene Synthesis, Characterization

and Its Applications: A Review, *Results Chem.*, 2021, **3**, 100163, DOI: 10.1016/j.rechem.2021.100163.

8 A. R. Urade, I. Lahiri and K. S. Suresh, Graphene Properties, Synthesis and Applications: A Review, *JOM*, 2023, **75**(3), 614–630, DOI: 10.1007/s11837-022-05505-8.

9 F. S. Irani, A. H. Shafaghi, M. C. Tasdelen, T. Delipinar, C. E. Kaya, G. G. Yapici and M. K. Yapici, Graphene as a Piezoresistive Material in Strain Sensing Applications, *Micromachines*, 2022, **13**(1), 119, DOI: 10.3390/mi13010119.

10 J. S. Meena, S. B. Choi, T. D. Khanh, H. S. Shin, J. S. Choi, J. Joo and J.-W. Kim, Highly Stretchable and Robust Textile-Based Capacitive Mechanical Sensor for Human Motion Detection, *Appl. Surf. Sci.*, 2023, **613**, 155961, DOI: 10.1016/j.apsusc.2022.155961.

11 X. Huang, G. Ge, M. She, Q. Ma, Y. Lu, W. Zhao, Q. Shen, Q. Wang and J. Shao, Self-Healing Hydrogel with Multiple Dynamic Interactions for Multifunctional Epidermal Sensor, *Appl. Surf. Sci.*, 2022, **598**, 153803, DOI: 10.1016/j.apsusc.2022.153803.

12 Y. Zhang, J. Yang, X. Hou, G. Li, L. Wang, N. Bai, M. Cai, L. Zhao, Y. Wang, J. Zhang, K. Chen, X. Wu, C. Yang, Y. Dai, Z. Zhang and C. F. Guo, Highly Stable Flexible Pressure Sensors with a Quasi-Homogeneous Composition and Interlinked Interfaces, *Nat. Commun.*, 2022, **13**(1), 1317, DOI: 10.1038/s41467-022-29093-y.

13 C. Hou, G. Tai, Y. Liu, R. Liu, X. Liang, Z. Wu and Z. Wu, Borophene Pressure Sensing for Electronic Skin and Human-Machine Interface, *Nano Energy*, 2022, **97**, 107189, DOI: 10.1016/j.nanoen.2022.107189.

14 Y. Du, W. Du, D. Lin, M. Ai, S. Li and L. Zhang, Recent Progress on Hydrogel-Based Piezoelectric Devices for Biomedical Applications, *Micromachines*, 2023, **14**(1), 167, DOI: 10.3390/mi14010167.

15 Q. He and J. Briscoe, Piezoelectric Energy Harvester Technologies: Synthesis, Mechanisms, and Multifunctional Applications, *ACS Appl. Mater. Interfaces*, 2024, **16**(23), 29491–29520, DOI: 10.1021/acsami.3c17037.

16 J. Lu, S. Hu, W. Li, X. Wang, X. Mo, X. Gong, H. Liu, W. Luo, W. Dong, C. Sima, Y. Wang, G. Yang, J.-T. Luo, S. Jiang, Z. Shi and G. Zhang, A Biodegradable and Recyclable Piezoelectric Sensor Based on a Molecular Ferroelectric Embedded in a Bacterial Cellulose Hydrogel, *ACS Nano*, 2022, **16**(3), 3744–3755, DOI: 10.1021/acsnano.1c07614.

17 Z. Ghemari, A. Bendaikha, S. Belkhiri and S. Saad, Fabrication of Flexible Resistive Pressure Sensors Using Graphene/Polydimethylsiloxane Composites, *Trans. Electr. Electron. Mater.*, 2025, **26**(3), 323–344, DOI: 10.1007/s42341-025-00601-3.

18 T. Gong, H. Zhang, W. Huang, L. Mao, Y. Ke, M. Gao and B. Yu, Highly Responsive Flexible Strain Sensor Using Polystyrene Nanoparticle Doped Reduced Graphene Oxide for Human Health Monitoring, *Carbon*, 2018, **140**, 286–295, DOI: 10.1016/j.carbon.2018.09.007.

19 S. P. Patole, S. K. Reddy, A. Schiffer, K. Askar, B. G. Prusty and S. Kumar, Piezoresistive and Mechanical Characteristics of Graphene Foam Nanocomposites, *ACS Appl. Nano Mater.*, 2019, **2**(3), 1402–1411, DOI: 10.1021/acsanm.8b02306.

20 J. Li, Z. Yuan, X. Han, C. Wang, Z. Huo, Q. Lu, M. Xiong, X. Ma, W. Gao and C. Pan, Biologically Inspired Stretchable, Multifunctional, and 3D Electronic Skin by Strain Visualization and Triboelectric Pressure Sensing, *Small Sci.*, 2022, **2**(1), 2100083, DOI: 10.1002/smsc.202100083.

21 S.-Y. Xia, Y. Long, Z. Huang, Y. Zi, L.-Q. Tao, C.-H. Li, H. Sun and J. Li, Laser-Induced Graphene (LIG)-Based Pressure Sensor and Triboelectric Nanogenerator towards High-Performance Self-Powered Measurement-Control Combined System, *Nano Energy*, 2022, **96**, 107099, DOI: 10.1016/j.nanoen.2022.107099.

22 Y. Xia Zhang, Y. He, Y. Liang, J. Tang, Y. Yang, H. Ming Song, M. Zrínyi and Y. Mei Chen, Sensitive Piezoresistive Pressure Sensor Based on Micropyramid Patterned Tough Hydrogel, *Appl. Surf. Sci.*, 2023, **615**, 156328, DOI: 10.1016/j.apsusc.2023.156328.

23 Y. Liu, T. Abdiryim, R. Jamal, X. Liu, N. Fan, M. Niyaz and Y. Zhang, High-Performance Quasi − Solid − State Hybrid Supercapacitor for Self − Powered Strain Sensor Based on Poly (3, 4 − Propylenedioxythiophene)/NiS2@Hollow Carbon Sphere Composite and Sulfonated Cellulose Hydrogel Electrolyte, *Appl. Surf. Sci.*, 2023, **608**, 154989, DOI: 10.1016/j.apsusc.2022.154989.

24 Y. Du, W. Du, D. Lin, M. Ai, S. Li and L. Zhang, Recent Progress on Hydrogel-Based Piezoelectric Devices for Biomedical Applications, *Micromachines*, 2023, **14**(1), 167, DOI: 10.3390/mi14010167.

25 Y. He, X. Y. Zhao, P. Rao, H. M. Song, Y. Yang, S. W. Sun, J. X. Zhou, Y. M. Chen, L. Tan and J. Z. Ma, Saline Tolerant Tough-yet-Strong Fiber-Reinforced Gel-Nacre for Soft Actuator, *Chem. Eng. J.*, 2022, **446**, 137091, DOI: 10.1016/j.cej.2022.137091.

26 Y. Sun, Z. Yu, Y. Gao, X. Ren, L. Duan and G. Gao, Flexible Hydrogel Sensor with Excellent Antibacterial and Low Temperature Frost Resistance, *Polymer*, 2023, **283**, 126282, DOI: 10.1016/j.polymer.2023.126282.

27 N. Nadeem, M. Sohail, M. H. Hassan Bin Asad, M. U. Minhas, Mudassir and S. A. Shah, Thermosensitive Hydrogels:From Bench to Market, *Curr. Sci.*, 2018, **114**(11), 2256, DOI: 10.18520/cs/v114/i11/2256-2266.

28 M. Vázquez-González and I. Willner, Stimuli-Responsive Biomolecule-Based Hydrogels and Their Applications, *Angew. Chem., Int. Ed.*, 2020, **59**(36), 15342–15377, DOI: 10.1002/anie.201907670.

29 X. Liu, Z. Huang, C. Ye, Z. Luo, L. Chen, X. Yao, F. Liang, T. Yang, H. Bi, C. Wang, C. Cai, L. Lyu and X. Wu, Graphene-Based Hydrogel Strain Sensors with Excellent Breathability for Motion Detection and Communication, *Macromol. Mater. Eng.*, 2022, **307**(8), 2200001, DOI: 10.1002/mame.202200001.

30 X. Xu, V. V. Jerca and R. Hoogenboom, Bioinspired Double Network Hydrogels: From Covalent Double Network Hydrogels via Hybrid Double Network Hydrogels to Physical Double Network Hydrogels, *Mater. Horiz.*, 2018, **5**(3), 408–415, DOI: 10.1039/C7MH01139C.

31 J. Zhang, Q. Huang and J. Du, Recent Advances in Magnetic Hydrogels, *Polym. Int.*, 2016, **65**(12), 1365–1372, DOI: 10.1002/pi.5170.

32 C. Wu, X. Huang, X. Wu, R. Qian and P. Jiang, Mechanically Flexible and Multifunctional Polymer-Based Graphene Foams for Elastic Conductors and Oil-Water Separators, *Adv. Mater.*, 2013, **25**(39), 5658–5662, DOI: 10.1002/adma.201302406.
33 H. Yao, J. Ge, C. Wang, X. Wang, W. Hu, Z. Zheng, Y. Ni and S. Yu, A Flexible and Highly Pressure-Sensitive Graphene–Polyurethane Sponge Based on Fractured Microstructure Design, *Adv. Mater.*, 2013, **25**(46), 6692–6698, DOI: 10.1002/adma.201303041.
34 Y. Lin, R. Yang and X. Wu, Recent Progress in the Development of Conductive Hydrogels and the Application in 3D Printed Wearable Sensors, *RSC Appl. Polym.*, 2023, **1**(2), 132–157, DOI: 10.1039/D3LP00077J.
35 J. N. Coleman, M. Lotya, A. O'Neill, S. D. Bergin, P. J. King, U. Khan, K. Young, A. Gaucher, S. De, R. J. Smith, I. V. Shvets, S. K. Arora, G. Stanton, H.-Y. Kim, K. Lee, G. T. Kim, G. S. Duesberg, T. Hallam, J. J. Boland, J. J. Wang, J. F. Donegan, J. C. Grunlan, G. Moriarty, A. Shmeliov, R. J. Nicholls, J. M. Perkins, E. M. Grieveson, K. Theuwissen, D. W. McComb, P. D. Nellist and V. Nicolosi, Two-Dimensional Nanosheets Produced by Liquid Exfoliation of Layered Materials, *Science*, 2011, **331**(6017), 568–571, DOI: 10.1126/science.1194975.
36 J. N. Israelachvili, Intermolecular and Surface Forces.
37 J. N. Coleman, Liquid-Phase Exfoliation of Nanotubes and Graphene, *Adv. Funct. Mater.*, 2009, **19**(23), 3680–3695, DOI: 10.1002/adfm.200901640.
38 S. Wang, Y. Zhang, N. Abidi and L. Cabrales, Wettability and Surface Free Energy of Graphene Films, *Langmuir*, 2009, **25**(18), 11078–11081, DOI: 10.1021/la901402f.
39 R. Mohammadi Sejoubsari, T. O. Xu, S. P. Ward, N. M. Bandara, Z. Zhang and D. H. Adamson, Electrically Conducting Porous Hydrogels by a Self-Assembled Percolating Pristine Graphene Network, *Soft Matter*, 2025, **21**(6), 1225–1232, DOI: 10.1039/D4SM01311E.
40 S. J. Woltornist, J.-M. Y. Carrillo, T. O. Xu, A. V. Dobrynin and D. H. Adamson, Polymer/Pristine Graphene Based Composites: From Emulsions to Strong, Electrically Conducting Foams, *Macromolecules*, 2015, **48**(3), 687–693, DOI: 10.1021/ma5024236.
41 W. D. Bancroft THE THEOliY OE' EMULSIFICATION, V.
42 M. J. Joyce, S. T. McDermott, K. Umaiya and D. H. Adamson, Polyphenol Modification of Graphene-Stabilized Emulsions to Form Electrically Conductive Polymer Spheres, *J. Colloid Interface Sci.*, 2024, **653**, 327–337, DOI: 10.1016/j.jcis.2023.09.008.
43 S. Zhao, S. Xie, Z. Zhao, J. Zhang, L. Li and Z. Xin, Green and High-Efficiency Production of Graphene by Tannic Acid-Assisted Exfoliation of Graphite in Water, *ACS Sustainable Chem. Eng.*, 2018, **6**(6), 7652–7661, DOI: 10.1021/acssuschemeng.8b00497.
44 T. Wang, L.-C. Jing, Q. Zhu, A. Sagadevan Ethiraj, X. Fan, H. Liu, Y. Tian, Z. Zhu, Z. Meng and H.-Z. Geng, Tannic Acid Modified Graphene/CNT Three-Dimensional Conductive Network for Preparing High-Performance Transparent Flexible Heaters, *J. Colloid Interface Sci.*, 2020, **577**, 300–310, DOI: 10.1016/j.jcis.2020.05.084.
45 G. Wang, Z. Chen, X. Jing, X. Yi, J. Zou, P. Feng, H. Zhang and Y. Liu, Ultrastable and Supersensitive Conductive Hydrogels Conferred by "Sodium Alginate Stencil" Anchoring Strategy, *Carbohydr. Polym.*, 2024, **335**, 122048, DOI: 10.1016/j.carbpol.2024.122048.
46 J. Zou, X. Jing, Z. Chen, S. Wang, X. Hu, P. Feng and Y. Liu, Multifunctional Organohydrogel with Ultralow-Hysteresis, Ultrafast-Response, and Whole-Strain-Range Linearity for Self-Powered Sensors, *Adv. Funct. Mater.*, 2023, **33**(15), 2213895, DOI: 10.1002/adfm.202213895.
47 Y. Zhao, J. Liu, Y. Hu, H. Cheng, C. Hu, C. Jiang, L. Jiang, A. Cao and L. Qu, Highly Compression-Tolerant Supercapacitor Based on Polypyrrole-mediated Graphene Foam Electrodes, *Adv. Mater.*, 2013, **25**(4), 591–595, DOI: 10.1002/adma.201203578.
48 M. J. Joyce, S. T. McDermott, K. Umaiya and D. H. Adamson, Polyphenol Modification of Graphene-Stabilized Emulsions to Form Electrically Conductive Polymer Spheres, *J. Colloid Interface Sci.*, 2024, **653**, 327–337, DOI: 10.1016/j.jcis.2023.09.008.
49 L. Qiu, J. Z. Liu, S. L. Y. Chang, Y. Wu and D. Li, Biomimetic Superelastic Graphene-Based Cellular Monoliths, *Nat. Commun.*, 2012, **3**(1), 1241, DOI: 10.1038/ncomms2251.
50 S. Zhao, Y. Gao, G. Zhang, L. Deng, J. Li, R. Sun and C.-P. Wong, Covalently Bonded Nitrogen-Doped Carbon-Nanotube-Supported Ag Hybrid Sponges: Synthesis, Structure Manipulation, and Its Application for Flexible Conductors and Strain-Gauge Sensors, *Carbon*, 2015, **86**, 225–234, DOI: 10.1016/j.carbon.2015.01.033.
51 P. Lv, K. Yu, X. Tan, R. Zheng, Y. Ni, Z. Wang, C. Liu and W. Wei, Super-Elastic Graphene/Carbon Nanotube Aerogels and Their Application as a Strain-Gauge Sensor, *RSC Adv.*, 2016, **6**(14), 11256–11261, DOI: 10.1039/C5RA20342B.
52 Y. Lu, W. He, T. Cao, H. Guo, Y. Zhang, Q. Li, Z. Shao, Y. Cui and X. Zhang, Elastic, Conductive, Polymeric Hydrogels and Sponges, *Sci. Rep.*, 2014, **4**(1), 5792, DOI: 10.1038/srep05792.
53 S. J. Woltornist, D. Varghese, D. Massucci, Z. Cao, A. V. Dobrynin and D. H. Adamson, Controlled 3D Assembly of Graphene Sheets to Build Conductive, Chemically Selective and Shape-Responsive Materials, *Adv. Mater.*, 2017, **29**(18), 1604947, DOI: 10.1002/adma.201604947.
54 S. J. Woltornist, A. J. Oyer, J.-M. Y. Carrillo, A. V. Dobrynin and D. H. Adamson, Conductive Thin Films of Pristine Graphene by Solvent Interface Trapping, *ACS Nano*, 2013, **7**(8), 7062–7066, DOI: 10.1021/nn402371c.
55 Z. Wang, Y. Tian, H. Liang, D. H. Adamson and A. V. Dobrynin, Electrical Conductivity of Graphene-Polymer Composite Foams: A Computational Study, *Macromolecules*, 2019, **52**(19), 7379–7385, DOI: 10.1021/acs.macromol.9b01669.
56 Z. Wang, H. Liang, D. H. Adamson and A. V. Dobrynin, From Graphene-like Sheet Stabilized Emulsions to Composite Polymeric Foams: Molecular Dynamics Simulations, *Macromolecules*, 2018, **51**, 7360–7367, DOI: 10.1021/acs.macromol.8b01082.

